

Thermally-induced qubit coherence in quantum electromechanics

N. Etehad Abari,^{1,*} A. Rakhubovsky,^{1,†} and R. Filip^{1,‡}

¹*Department of Optics, Palacký University, 17. Listopadu 12, 771 46 Olomouc, Czech Republic*

(Dated: June 10, 2022)

Quantum coherence, the ability of a quantum system to be in a superposition of orthogonal quantum states, is a distinct feature of the quantum mechanics, thus marking a deviation from classical physics. Coherence finds its applications in quantum sensing and metrology, quantum thermodynamics and computation. A particularly interesting is the possibility to observe coherence arising in counter-intuitive way from thermal energy that is without implementation of intricate protocols involving coherent driving sequences. In this manuscript, we investigate quantum coherence emerging in a hybrid system composed of a two-level system (qubit) and a thermal quantum harmonic oscillator (a material mechanical oscillator), inspired by recent experimental progress in fabrication of such systems. We show that quantum coherence is created in such a composite system solely from the interaction of the parts and persists under relevant damping. Implementation of such scheme will demonstrate previously unobserved mechanisms of coherence generation and can be beneficial for hybrid quantum technologies with mechanical oscillators and qubits.

I. INTRODUCTION

Coherence is a fundamental concept in quantum mechanics that is connected to the superposition of quantum states in a basis preferred for a certain application. Quantum states that possess this non-zero coherent superposition of basis states can provide advantage for science and technology over the incoherent statistical mixtures of the same basis states. Coherence enhances performance of the quantum protocols in sensing and metrology [1, 2], quantum thermodynamics [3, 4], and quantum information processing [5–7]. Quantum coherence has been shown to play a role in biological processes as well [8, 9]. In order to quantify the coherence, a few resource theories have been put forward [10–13]. Interplay between coherence and other quantum resources such as entanglement, discord and steering has been investigated in [14, 15]. On the other hand, it remains unexplored how quantum coherence emerges during quantum dynamics from incoherent thermal states.

Generally, quantum coherence of an open system emerges in presence of an external strong coherent drive. Recently, it has been shown [16] that quantum coherence can emerge in a steady state of a system that only interacts with its environment given certain properties of this interaction. Subsequent studies proposed similar system-environment phenomena [17–22]. In parallel, an experimental proposal in double-quantum-dot solid-state systems was analyzed [23]. However, even proof-of-principle experimental tests of such phenomena are still missing due to the challenging engineering of composite interactions.

In our work we investigate coherence emerging in a hybrid electromechanical system similar to the one studied in [24]. We show that coherence in each subsystem can emerge solely from coherent interaction between the constituents that start from fully incoherent states. We analyze such thermal rise of quantum coherence in quantum electromechanics and propose an experiment to observe the principle mechanism. Moreover, we describe a regime where thermal mechanical oscillator monotonously stimulates qubit coherence, even if the phonon number is much larger than unity. Hybrid systems such as this combine benefits of the constituents allowing the positive synergy to open new perspectives in science and technology. Electromechanical systems, by combining advantages of superconducting devices and high-Q mechanical oscillators, allow preparation of exotic states of macroscopic mechanical oscillators [24, 25], and transduce quantum information between microwave and optical domains [26, 27]. Such transduction not only allows an effective long-range communication between superconducting devices but also their effective readout by optical means [28].

II. RESULTS

A. Model of the qubit-mechanical system

In this manuscript, we demonstrate a possibility to generate coherence in a coupled system of nanomechanical oscillator and a two-level system (a qubit) from a fully incoherent state. A schematic depiction of the scheme is in Fig. 1 (a). First, we introduce

* Corresponding author: najmeh.etehadiabari@upol.cz

† rakhubovsky@optics.upol.cz

‡ filip@optics.upol.cz

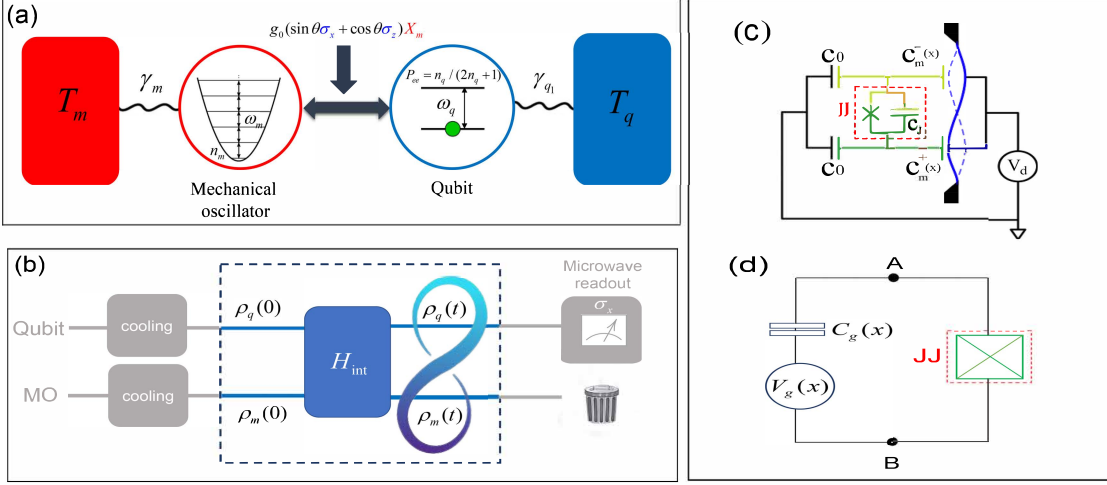


FIG. 1. (a) Schematic diagram of the physical system. A single-mode mechanical harmonic oscillator of frequency ω_m is coupled to a qubit (frequency ω_q) via a general coupling rate g_0 . (b) A sketch of the interaction protocol between the qubit and the mechanical mode. Before the interaction, the qubit and the mechanical oscillator are prepared in the incoherent states, respectively, $\rho_q(0)$ and $\rho_m(0)$, either by cooling, or by equilibration with the corresponding bath. The quantum coherence is evaluated after the interaction has finished, and can be probed by microwave readout. (c) An experimental illustration of the model consisting of a charge qubit (CPB) coupled to the mechanically compliant capacitors in an electromechanical system [24]. The red-dashed rectangle area indicates the Josephson Junction (JJ) represented by a nonlinear inductor and a Josephson capacitor C_J . The suspended superconducting islands of the CPB which connect the charge qubit to the superconducting reservoir (other parts of the circuit) are displayed in light and dark green colors. The motion of the mechanical oscillator (blue electrodes) can modify the separation between the two capacitors $C_m^\pm(x)$ which are modulated with the opposite phase by the anti-symmetric motion of the mechanical oscillator (MO). V_{dc} characterizes the DC-voltage applied to the MO. The gate-charge (offset charge) $n_g = C_g(x)V_g(x)/2$ applying on the CPB, can be defined by the equivalent capacitor $C_g(x)$ and voltage $V_g(x)$ of the circuit which are now position-dependent (see Appendix A). The modulation of the offset charge via the mechanical motion induces a coupling between the mechanical motion and qubit-electrostatic energy. (d) The equivalent circuit of the experimental model.

a theoretical description of the system and the figures of merit. The electromechanical systems of interest, akin to investigated in [24], can be described by the Hamiltonian ($\hbar \equiv 1$)

$$H = \frac{\omega_q}{2} \sigma_z + \frac{\omega_m}{2} (X_m^2 + P_m^2) + \sqrt{2} g_0 (\sin \theta \sigma_x + \cos \theta \sigma_z) X_m. \quad (1)$$

Here the first two terms describe the free dynamics of the qubit (with Pauli matrices σ_i and transition frequency ω_q) and the nanomechanical oscillator (with eigenfrequency ω_m and the dimensionless position and momentum quadratures, respectively, X_m and P_m normalized such that $[X_m, P_m] = i$). For convenience, we also define the detuning $\Delta = \omega_q - \omega_m$. The third term in (1) describes the interaction between the qubit and mechanics required to achieve emerging quantum coherence [16]. We focus on proof-of-principle demonstration of the interaction mechanism using only one dominant mode at the frequency ω_m coupled to an external bath. From a thermal occupation of the qubit, this composite interaction can generate a coherent displacement of the oscillator, continuously generating quantum coherence in the qubit. In an experiment the hybrid interaction can be realized via capacitive, magnetic flux or electromotive coupling methods [29]. The coupling can be tuned in magnitude by changing the rate g_0 or adjusted by manipulating the value of θ . This can be advantageously reached by utilizing the suitable lumped elements in the superconducting circuit [24, 29, 30] since in our model θ depends on the charging and Josephson energies while g_0 can be controlled through DC voltage bias and capacitors of the circuit as well as charging energy (see Fig. 1(c,d) and Appendix A for more details).

To investigate emerging coherence in such system, we assume that both mechanics and qubit are prepared initially in thermal states, states that lack coherence in the natural basis of Fock states. The initial state of the compound system therefore reads

$$\rho(0) = \rho_{\text{qubit}}(0) \otimes \rho_m(0) = (P_{ee}|e\rangle\langle e| + (1 - P_{ee})|g\rangle\langle g|) \otimes \sum_{k=0}^{\infty} \frac{n_m^k}{(1 + n_m)^{k+1}} |k\rangle\langle k|, \quad (2)$$

where $|g\rangle$ [$|e\rangle$] is the ground [excited] state of the qubit, $|k\rangle$ is a Fock state of the mechanical oscillator, $P_{ee} = n_q/(2n_q + 1)$. The mean occupation number of mechanics n_m and the occupation parameter n_q of the qubit obey Bose-Einstein statistics: $n_i = [\exp(\hbar\omega_i/k_B T_i) - 1]^{-1}$ for $i = q, m$, with k_B being the Boltzmann constant and T_i the temperature of the corresponding subsystem.

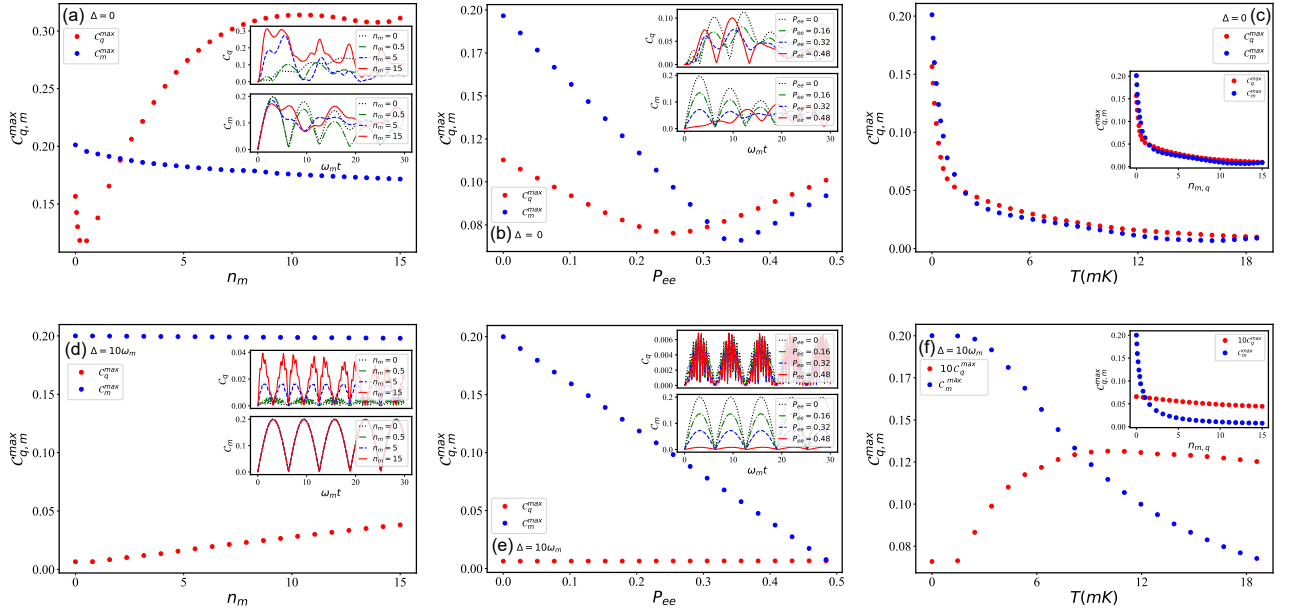


FIG. 2. Maximally attainable coherence C_q and mechanical displacement C_m as a function of the initial occupation of mechanics (a,d) or qubit (b,e) given a constant initial occupation of the other subsystem. In (a,d) the qubit is initially in the ground state $P_{ee} = 0$. In (b,e) the mechanics has initial occupation $n_m = 0.5$. Insets show the evolution of C_q and C_m as functions of time for different occupation. Note that C_q and C_m assume their corresponding maximal values at different instants of time. (c,f) Optimum values of C_q, C_m as a function of the initial temperature assuming equal temperature baths for both subsystems. The inset plots of panels (c,f) show how C_q^{\max}, C_m^{\max} change as a function of equal initial occupation (in this case, the initial temperatures differ in panel (f)). In each panel, weak coupling regime $g_0 = 0.1\omega_m$ is assumed. The panels (a,b,c) correspond to the resonance between the qubit and MO ($\omega_m = \omega_q$); in (d,e,f) $\omega_q - \omega_m = \Delta = 10\omega_m$.

The dynamics generated by the Hamiltonian (1) is capable of driving the initially incoherent state (2) into a state in which both mechanics and the qubit possess quantum coherence. From a plethora of available measures of coherence (see Ref. [11] for a review), we choose the l_1 -norm-based measure [31] to quantify the qubit coherence. This measure has the meaning of mean displacement in xy -plane and can be computed for the qubit as

$$C_q = \sqrt{\langle \sigma_x \rangle^2 + \langle \sigma_y \rangle^2}. \quad (3)$$

Throughout the manuscript we will compare the qubit's coherence with the mean coherent displacement of the oscillator $C_m = \sqrt{\langle X_m \rangle^2 + \langle P_m \rangle^2}$. Note that in general the l_1 -norm such as displacement is not a proper coherence monotone for an oscillator (a system with infinite-dimensional Hilbert space) as it can diverge on states with finite mean energy [32]. Nevertheless, the mean coherent displacement is an illustrative quantity that can provide a quantum advantage in e.g. metrology. The mean values in Eq. (3) are computed over the evolved quantum state $\rho(t)$. In the case of unitary dynamics, $\rho(t) = e^{-iHt}\rho(0)e^{iHt}$. In a realistic case where both systems are subject to decoherence caused by interaction with the corresponding environment, one has to use more complicated tools, such as solving master equation (see Section IV for elaboration).

B. Quantum coherence generated by pulsed noiseless dynamics

The simple model of the Hamiltonian (1) captures a rich dynamics whose exact type depends on the interplay between the eigenfrequencies of individual subsystems $\omega_{m,q}$ and the coupling defined by its magnitude g_0 and phase θ . Moreover, generation of coherence in this system is determined by the initial state before the interaction starts. In this subsection, we show that, counterintuitively, increasing temperature of the initial quantum state can be beneficial for generation of coherence in the qubit. To estimate the limits of attainable values of coherence, we start with the noiseless case when the two subsystems, the MO and the qubit are decoupled from their environments and only couple to each other.

In order to see the effect of the initial thermal occupation on the coherence generation, we simulate the dynamics of the system driven by only the Hamiltonian (1) and ignore the coupling to the environment. In this case, the quantum state of the bipartite system after the interaction can be obtained straightforwardly by applying unitary transformation to the initial product state (2). The estimates of the coherence emerging from the unitary qubit-mechanical interaction are shown at Fig. 2. The numerical study

assumes weak coupling regime $g_0 = 0.1\omega_m \ll \omega_m + \omega_q$, and $\theta = \pi/4$, equal coupling of mechanical displacement to both σ_x and σ_z , in order to gain the optimum values of the coherence parameters (the dependence of the coherence parameters to θ , i.e., coupling rates g_x, g_z , as well as the absolute value of the qubit-mechanical coupling g_0 and the detuning Δ is discussed in more details in Sec. II C).

As seen in Fig. 2(a,d), having a hotter initial mechanical state has a positive effect on qubit coherence such that by increasing the mechanical temperature or equivalently increasing thermal occupation n_m , we reach higher maximum values for C_q^{\max} . The duration of time it takes to reach the maximal value C_q^{\max} is also reduced with increasing initial occupation n_m , which is illustrated by the inset plots. This phenomenon contrasts with a steady-state qubit coherence induced by a multimode bosonic bath [16, 21, 23], where the maximum of coherence appears for vanishing temperature. Interestingly, the increase in coherence is accompanied by only a moderate coherent displacement decrease in the oscillator. The opposite happens when the qubit's initial temperature is increased at $\Delta = 0$ when we fix the value of $n_m = 0.5$. As seen in Fig. 2(b) the maximum accessible amounts of C_q can be reached when $P_{ee} = 0$, i.e., $n_q = 0$. Elevated initial occupations of the qubit do not significantly alter the qubit coherence C_q in the dispersive regime $\Delta = 10\omega_m$. Therefore, it is advantageous to keep the qubit initially in the ground state and increase the oscillator's initial temperature to observe emerging quantum coherence, more significant than the steady-state coherence [16, 21, 23].

The optimum values of C_m show a slow reduction as a function n_m for $\Delta = 0$, while in the dispersive regime the maximum values of C_m^{\max} do not change considerably with respect to n_m (compare Fig. 2(a,d), blue dots, and inset plots for C_m). In addition, by increasing the detuning and moving from the resonance case to the off-resonance one, the decrease rate of C_m^{\max} becomes faster when the qubit temperature rises (compare Fig. 2(b,e), blue dots, and inset plots for C_m).

Finally, for the case in which the initial temperatures of the qubit and the MO are equal ($T_m = T_q = T$), the maximum attainable amounts of C_q and C_m are shown in panels (c) and (f) of Fig. 2, for resonance and off-resonance cases, respectively. Inset plots of Fig. 2(c,f) also demonstrate the optimum values of coherence parameters as a function of the initial occupation assumed equal for both subsystems ($n_q = n_m = n_{m,q}$). As is seen, by increasing the thermal occupation numbers of two subsystems at the same time, i.e., increasing $n_{m,q}$, C_q^{\max} , and C_m^{\max} decrease (the reduction rate of the C_q^{\max} as a function of $n_{m,q}$ is not significant in dispersive regime $\Delta = 10\omega_m$). For the case of resonance, the results of the inset plots are the same as the main plot (c), as $\omega_m = \omega_q$ and $T_m = T_q = T$ give us the identical occupations $n_m = n_q = n_{m,q}$. However, at $\Delta = 10\omega_m$, the main plot of Fig. 2(f) for C_q^{\max} shows a small increase as the temperature of the baths rises simultaneously. Therefore, we can conclude that as long as $n_q < n_m$, by raising the temperature, it is possible to observe an increase of the value of the qubit coherence parameter.

In addition, by comparing the first row and the second row of Fig. 2, we realize that by increasing the detuning, the energy exchange between the mechanical mode and qubit through the coupling channel $g_x = g_0 \sin \theta$ reduces, which causes the reduction in maximum accessible amount of qubit coherence since C_q depends on both g_x and $g_z = g_0 \cos \theta$ (see Sec. II C for further details). On the other hand, as C_m is only influenced by coupling rate g_z , increasing the detuning does not affect the maximum reachable amount of C_m^{\max} .

C. Effect of the interaction parameters on the coherence generation

To demonstrate the effects of the coupling rates g_x and g_z on the generation of quantum coherence in the system, in first and second columns of Fig. 3, we showed the evolution of coherence parameters C_q and C_m in time and with respect to θ , in weak coupling regime $g_0 = 0.1\omega_m$, for resonance ($\Delta = 0$) and off-resonance ($\Delta = 10\omega_m$) conditions, respectively. For both cases, the maximum oscillator displacement rises at $\omega_m t = \pi$, but the maximum qubit coherence appears delayed at resonance in Fig. 3 (a,b). Out-of-resonance, in Fig. 3 (d,e), both displacement and coherence appear synchronously.

As is seen from Fig. 3(a,d), the qubit coherence parameter $C_q(t)$ takes the non-zero value when $\theta \neq n\pi/2$ ($n = 1, 2, \dots$), i.e., when both $g_x, g_z \neq 0$. The maximum amount of $C_q(t)$ can be obtained for $\theta = (2n+1)\pi/4$, which shows that C_q strongly depends on the factor $|g_x g_z| = |g_0^2 \sin(2\theta)/2|$. In addition, increasing the detuning causes a fast reduction in the maximum available amounts of qubit coherence C_q (compare panels (a) and (d) in Fig. 3). Moreover, at resonance, the evolution of $C_q(t)$ becomes maximized around $t \approx 2m\pi/\omega_m$ ($m \in \mathbb{N}$), whereas at $\Delta = 10\omega_m$, the interference pattern shows itself in shorter time interval and the maximum values of C_q shift to smaller time interval $2\pi/3 < \omega_m t < 4\pi/3$.

On the other hand, for the fixed values of $g_0 = 0.1\omega_m$, $n_m = 0.5$ and $n_q = 0$, the mechanical displacement $C_m(t)$ is not influenced by changing the detuning (see Fig. 3(b,e)) and is only affected by the displacement coupling rate $g_z = g_0 \cos \theta$. Therefore, the maximum amount of C_m is achieved when $\theta = (2n+1)\pi/2$ and $t \approx (2m-1)\pi/\omega_m$.

In Panels (c) and (f) of Fig. 3, the maximum values of dynamical coherence parameters are depicted as a function of absolute qubit-mechanical coupling g_0/ω_m which shows that the stronger coupling gives rise to higher quantum coherence in the system.

The dependence of the mean values of the mechanical quadratures $\langle X_m(t) \rangle$ and $\langle P_m(t) \rangle$ on g_z and the Pauli matrices $\langle \sigma_x(t) \rangle$ and $\langle \sigma_y(t) \rangle$ on both g_x and g_z can also be revealed analytically for a very short time interval in ideal evolution where we can approximate the time evolution operator $U(t) = e^{-iHt} \approx \mathbb{I} - iHt$. Therefore, the final state of the system up to second order in

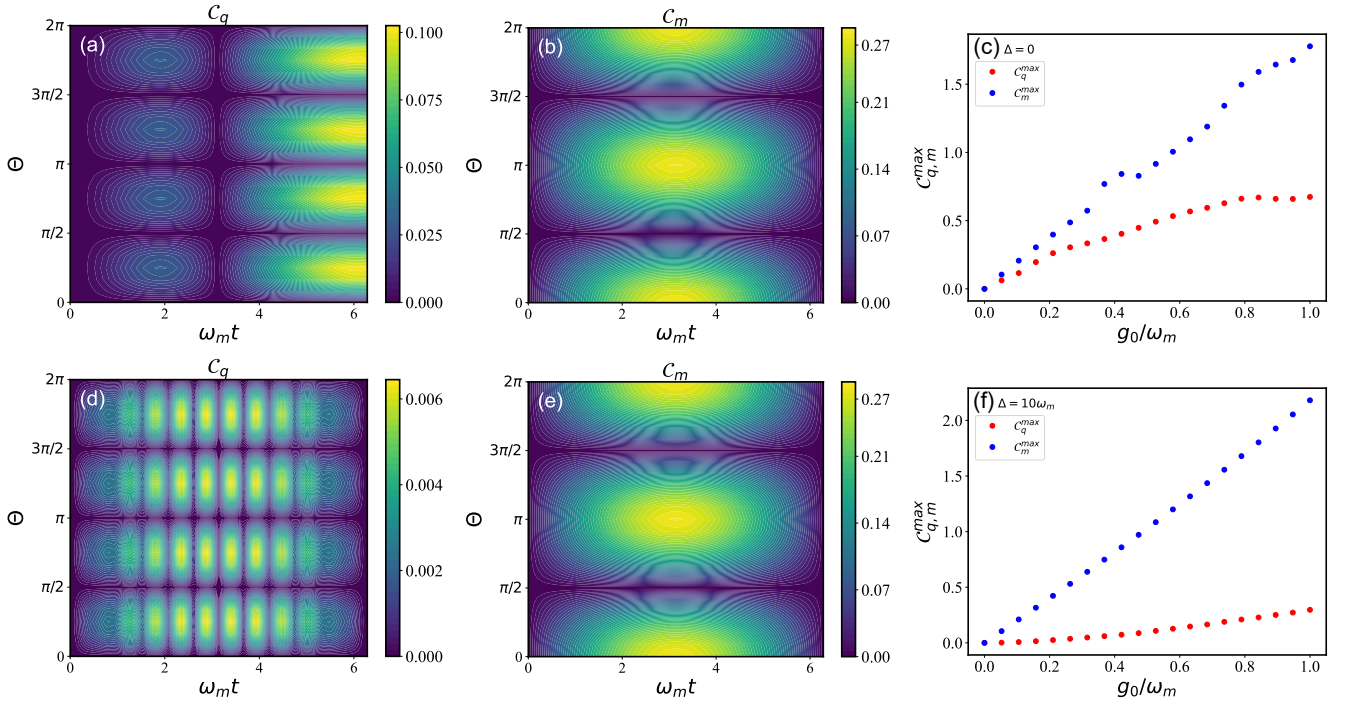


FIG. 3. Coherence dynamics caused by qubit-oscillator interaction: (a,b,d,e) The contour plots of the coherence parameters C_q and C_m with respect to the normalized time $\omega_m t$ and θ when $g_0 = 0.1\omega_m$. (c,f) The maximal attainable values of the quantum coherence as a function of normalized qubit-mechanical coupling g_0/ω_m for $\theta = \pi/4$. In (a-c) $\Delta = 0$, in (d-f) $\Delta = 10\omega_m$. Other parameters are $n_q = 0$ and $n_m = 0.5$: the qubit is initialized in its ground state while the MO is in a thermal state.

time is given by

$$\rho_f(t) \approx \rho(0) - it [H, \rho(0)] + t^2 H \rho(0) H + \mathcal{O}(t^2). \quad (4)$$

Under such approximation, the system operators' mean values become

$$\langle X_m(t) \rangle \approx \sqrt{2}g_z t^2 \left[\omega_m n_m (4n_m + 3)(2P_{ee} - 1) + \frac{\omega_q}{2}(2n_m + 1) \right], \quad (5a)$$

$$\langle P_m(t) \rangle \approx -\sqrt{2}g_z t (2P_{ee} - 1), \quad (5b)$$

$$\langle \sigma_x(t) \rangle \approx 2g_x g_z t^2 (2n_m + 1)(2P_{ee} - 1), \quad (5c)$$

$$\langle \sigma_y(t) \rangle \approx 0. \quad (5d)$$

where $P_{n,n} = n_m^n / (1 + n_m)^{n+1}$ denotes coefficients of expansion of the initial thermal state of the mechanics in the Fock-state basis, n_m is this state's mean occupation. From Eq. 5, we see that up to $\mathcal{O}(t^2)$, the mechanical quadratures $\langle X_m(t) \rangle$ and $\langle P_m(t) \rangle$ are only affected by g_z . However, $\langle \sigma_x(t) \rangle$ and therefore, C_q depends on the product $g_x g_z$. From Eqs. (5c) and (5d), we obtain $C_q \approx |\langle \sigma_x(t) \rangle| = 2|g_x g_z| t^2 (2n_m + 1) / (2n_q + 1)$. This indicates that in short time interval, C_q changes quadratically with time ($C_q \propto t^2$). The qubit coherence C_q also depends on the mechanical and the qubit occupation number ratio $C_q \propto (2n_m + 1) / (2n_q + 1)$ which reveals why we could attain better results of C_q^{\max} when $n_q < n_m$ (see Fig. 2). Hence, the best result can be achieved when we fix $n_q = 0$, while increasing the initial occupation n_m (see Fig. 2). While the short-time approximation agrees qualitatively with simulations, the quantitative agreement holds only for very short times $\omega_m t \ll 1$. The maximal values of coherence are reached at considerably longer times which, unfortunately, do not admit the analytical solution.

It is also worth looking at the variations of the quantum coherence with respect to the detuning to investigate the resonant nature of this phenomenon. The optimum values of coherence parameters C_q^{\max} and C_m^{\max} as a function of normalized detuning Δ/ω_m have been demonstrated in Fig. 4(a), where we can detect a maximum peak for C_q^{\max} around $\Delta/\omega_m \approx 0$. However, the maximum amounts of the mechanical coherent displacement C_m^{\max} won't alter much as a function of detuning which is consistent with Fig. 3(b,e) when we fix the values of $g_0 = 0.1\omega_m$, $\theta = \pi/4$, $n_m = 0.5$ and $n_q = 0$.

In addition, in panels (b,c) of Fig. 4, we showed the evolution of C_q and C_m , respectively, for different values of normalized detuning. As is seen in panel (b), by changing the detuning from $\Delta = -0.5\omega_m$ to $\Delta = 10\omega_m$ and moving to the dispersive regime,

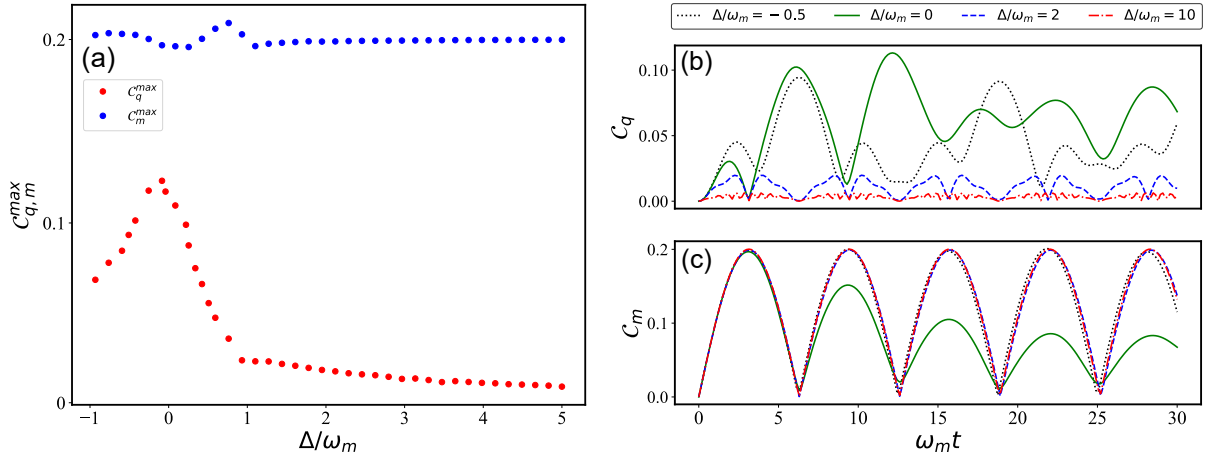


FIG. 4. Resonant features of emergent quantum coherence: (a) Optimum values of the coherence parameters as a function of the normalized detuning Δ/ω_m . The definition of the detuning $\Delta = \omega_q - \omega_m$ does not allow values below $-\omega_m$. The evolution of (b) the qubit coherence $C_q(t)$ and (c) the mechanical coherent displacement $C_m(t)$ for different values of detuning. Other numerical parameters are $g_0 = 0.1\omega_m$, $\theta = \pi/4$, $n_m = 0.5$, and $n_q = 0$.

the amplitude of C_q diminishes fast. On the other hand, the oscillation amplitude of C_m becomes maximized for the initial time interval, and increasing the detuning doesn't change it (see Fig. 4(c)).

To find out why the coherence parameters respond to the detuning like what is mainly shown in Fig. 4, it would be better to take a look at the Hamiltonian of the system in the interaction picture, given by

$$H^{(I)} = e^{+iH_0 t} H e^{-iH_0 t} - H_0 = g_x(\sigma_- a^\dagger e^{-i\Delta t} + \sigma_+ a e^{+i\Delta t}) + g_x(\sigma_+ a^\dagger e^{i\Sigma t} + \sigma_- a e^{-i\Sigma t}) + g_z \sigma_z (a^\dagger e^{+i\omega_m t} + a e^{-i\omega_m t}), \quad (6)$$

where $a = (X_m + iP_m)/\sqrt{2}$ denotes the mechanical annihilation operator, and $\Sigma = \omega_q + \omega_m$. From Eq. (6), we can see that for $\Delta \approx 0$, the rotating terms $g_x(\sigma_- a^\dagger + \sigma_+ a)$, which are responsible for an exchange of excitations between the qubit and the MO, play the dominant role in the dynamics of the system, more specifically in C_q through the coupling channel g_x . By increasing the absolute value of the detuning, both the rotating and counter-rotating terms in Eq. (6) start oscillating fast with the frequency of Δ and Σ , respectively. In the dispersive regime, where $\Sigma > \Delta \geq 10\omega_m$, and due to the adiabatic evolution, the energy exchange between the qubit and the MO which mainly happens through the coupling channel g_x diminishes. This affects the qubit coherence which depends on both g_x and g_z factors and leads us to the smaller maximum amounts of C_q . As the mechanical coherent displacement is mainly influenced by the coupling rate g_z and therefore, the displacement term $g_z \sigma_z (a^\dagger e^{+i\omega_m t} + a e^{-i\omega_m t})$, changing the detuning can not significantly impact C_m (see Fig. 3(b,e) and Fig. 4(a,c)).

D. Quantum coherence in the presence of damping and noise

In order to study the dynamics of the system more realistically, we need to take the dissipation and decoherence effects into account. For an open system interacting with an environment, its density matrix obeys the Lindblad master equation

$$\dot{\rho} = -i[H, \rho] + \frac{\gamma_m}{2}(n_m + 1)\mathcal{L}(a)\rho + \frac{\gamma_m}{2}n_m\mathcal{L}(a^\dagger)\rho + \frac{\gamma_{q_1}}{2}(n_q + 1)\mathcal{L}(\sigma_-)\rho + \frac{\gamma_{q_1}}{2}n_q\mathcal{L}(\sigma_+)\rho \quad (7)$$

Here, $\mathcal{L}(O) = 2O\rho O^\dagger - (O^\dagger O\rho + \rho O^\dagger O)$ ($O \equiv a, a^\dagger, \sigma_\pm$) denotes the Lindblad superoperator. Further, $\gamma_m, \gamma_{q_1} = 1/T_1$ represent the mechanical and qubit relaxation rates, respectively. By solving the master equation (7) numerically, we have investigated the effects of the mechanical and qubit damping on the dynamics of coherence parameters for resonance case $\Delta = 0$ (see Fig. 5).

In panel (a) of Fig. 5, we showed the changes of the attainable quantum coherence with respect to the mechanical damping rates γ_m/ω_m in the absence of the qubit dissipation and noise ($\gamma_{q_1} = n_q = 0$) and when the system is operated in resonance condition $\Delta = 0$ and weak coupling regime $g_0 = 0.1\omega_m$. We also consider the mechanical occupation to be $n_m = 0.5$. As can be seen in Fig. 5(a), the maximum values of coherence parameters C_q^{\max} and C_m^{\max} do not change considerably as γ_m/ω_m increases. In addition, it is evident from the inset plots of Fig. 5(a) that the dynamical coherence parameters overlap for all $\gamma_m/\omega_m < 10^{-2}$ which means that they are completely robust against mechanical damping as far as $\gamma_m/\omega_m < 10^{-2}$. Moreover, larger values of the mechanical dissipation such as $\gamma_m/\omega_m = 10^{-2}$, do not affect the coherence parameters for the initial time interval (red dotted-dashed lines in inset plots of Fig. 5(a)). However, we could observe decrease of the coherence parameters for a longer time. By comparing the inset plots in 5(a), we realize that C_q decreases with the faster rate than C_m for $\gamma_m/\omega_m = 10^{-2}$.

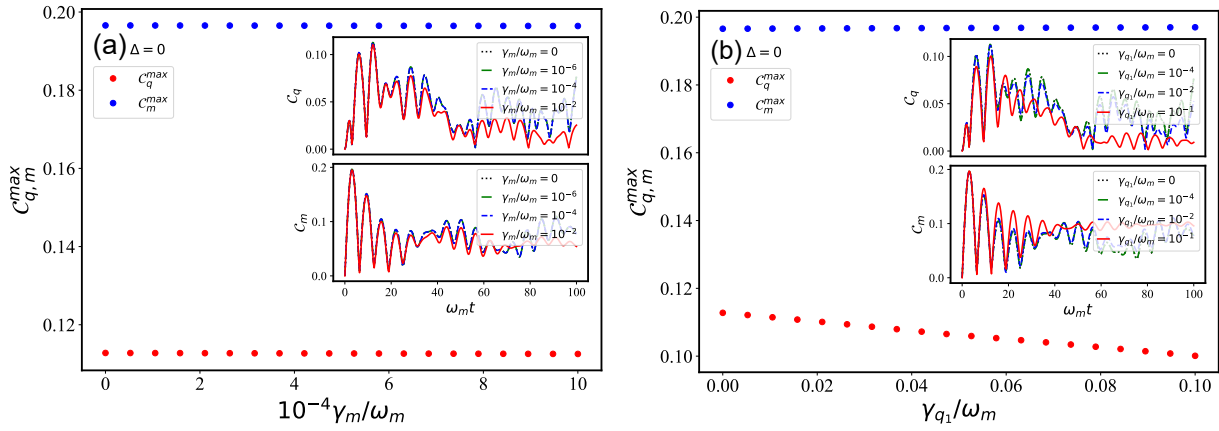


FIG. 5. Robustness of emerging quantum coherence: optimum values of the coherence parameters as a function of the normalized (a) mechanical damping rate γ_m/ω_m when $\gamma_{q_1}/\omega_m = 0$ and (b) qubit damping rate γ_{q_1}/ω_m for $\gamma_m/\omega_m = 10^{-6}$. Inset plots show the evolution of the coherence parameters for different values of (a) γ_m/ω_m and (b) γ_{q_1}/ω_m . Other numerical parameters are $\Delta = 0$, $g_0 = 0.1\omega_m$, $n_m = 0.5$, and $n_q = 0$.

The evolution of the coherence parameters in the presence of the normalized qubit damping rate γ_{q_1}/ω_m is plotted in Fig. 5(b) when we consider $n_m = 0.5$, $n_q = 0$ and $\gamma_m/\omega_m = 10^{-6}$. In this case, we can see that C_q^{\max} decreases with increasing qubit relaxation rate, while C_m^{\max} does not change much with increasing γ_{q_1}/ω_m which emphasizes the robustness of mechanical displacement against qubit damping. The inset plots also confirm these results. In addition, by looking to the inset plots of Fig. 5(b), it is clear that for $\gamma_{q_1}/\omega_m = 10^{-2}$, coherence parameters would be resistant to the qubit dissipation in shorter time interval $\omega_m t \leq 2\pi$. Simulations in the longer time interval show that both C_q and C_m decrease and eventually reach small non-zero steady-state values ($C_q \approx 0.01$, $C_m \approx 0.1$).

To summarize our study of the influence of the baths, the maximum of attainable coherence seems to be reached at rather early times that amount to the interaction running for only a few periods of mechanical oscillations. For the state-of-the-art electromechanical systems, due to their exceptional Q-factors, the interaction at these timescales is very close to unitary. Therefore, we can state that the interaction with thermal reservoirs during the coherent interaction between the mechanics and the qubit, has very limited effect on the maximal coherence attainable from fast pulsed interaction studied here.

III. DISCUSSION

In this article, in contrast to the previous steady-state studies [16, 19] we theoretically investigated the possibility of generating transient quantum coherence in a qubit-mechanical system from incoherent thermal states. We studied the transient interaction between a charge qubit and a mechanical oscillator, similar to what is found in electromechanical setups [24, 25, 33–37]. We showed how the sensitivity of the qubit to the offset charge enables us to couple the qubit to the mechanical motion in both vertical and parallel ways with respect to the eigenstates of the free Hamiltonian of the qubit as far as the system is operated near the degeneracy point. The simultaneous presence of these two different coupling rates allows the observation of the qubit coherence in the system with the initial incoherent thermal state. This is so in both the ideal case of unitary interaction and in the dissipative situation. It should be noted that in this model, dynamical coherence emerges without the use of conventional methods such as coherent driving [38] or coherence measurement [39, 40].

Differently to the steady-state coherence, the thermal occupation number of the mechanical mode has a positive effect on generating larger coherence of the qubit. We observed that increasing the net values of the coupling rate g_0 causes an improvement in the maximum accessible amounts of the qubit coherence and mechanical coherent displacement. In addition, we demonstrated how the parallel and perpendicular components g_z and g_x of the coupling rates affect the quantum coherence. In the case of the qubit coherence C_q , the product $g_x g_z$ plays the main role while for mechanical displacement C_m , the parallel coupling g_z becomes important. The maximum coherence values for the qubit and the MO could be obtained for $|g_x| = |g_z|$, i.e., when we set the optimum value $\theta = \pi/4$ for the coupling phase. Moreover, we showed that the qubit coherence parameter is strongly dependent on the detuning Δ through the coupling channel g_x such that by adjusting the detuning and setting it close to resonance $\Delta \approx 0$, where the role of the rotating term associated with the coupling rate g_x gets dominant, we reach the maximum values for the qubit coherence parameter. However, changing the detuning can not significantly alter the maximum values of mechanical displacement. Finally, we obtained that the mechanical coherence generated in our model is almost robust against both the mechanical and the qubit damping processes, while the larger values of qubit damping rate ($\gamma_{q_1} > 10^{-2}\omega_m$) give rise to

the decaying of the qubit coherence parameter.

The experimental realization of such a model has been already demonstrated in Ref. [24]. Aside from the electromechanical setups, there are other experimental platforms for the realization of our model such as trapped ions [41, 42] and NV-centers coupled magnetically to the mechanical motion [43–45]. Hybrid atom-optomechanical and electro-optomechanical systems also provide a great potential for this purpose [46–51].

Quantum coherence counts among fundamental resources in quantum information processing and quantum computation [10, 11, 52]. It also provides great applications in the context of quantum sensing [53], quantum thermodynamics [54–56], quantum biology [8] and non-equilibrium models [4, 57, 58]. In each of these fields, autonomous emergence of quantum coherence can be beneficial. Such proof-of-principle experimental tests will further investigate the emergence of quantum coherence and extensions of the mechanisms we addressed here.

IV. METHODS

A. Tools for numerical calculation

In this manuscript, we use the QuTiP package [59, 60] to numerically investigate the evolved density matrix as well as coherent properties of the system in both ideal and dissipative situations. For the ideal case, we solve the von Neumann equation $\dot{\rho}(t) = -i[H, \rho]$ with the initial condition (2). However, the total density matrix in an open system is obtained by solving the master equation

$$\dot{\rho} = -i[H, \rho] + \sum_n \frac{1}{2} \left(2\mathcal{A}_n \rho(t) \mathcal{A}_n^\dagger - \rho(t) \mathcal{A}_n^\dagger \mathcal{A}_n - \mathcal{A}_n^\dagger \mathcal{A}_n \rho(t) \right), \quad (8)$$

numerically, where in our system $\mathcal{A}_1 = \sqrt{\gamma_m(n_m + 1)} a$, $\mathcal{A}_2 = \sqrt{\gamma_m n_m} a^\dagger$, $\mathcal{A}_3 = \sqrt{\gamma_{q_1}(n_q + 1)} \sigma_-$ and $\mathcal{A}_4 = \sqrt{\gamma_{q_1} n_q} \sigma_+$. As mentioned before, the Hamiltonian H appearing in von Neumann and master equations is given by

$$H = H_0 + H_{int}, \quad (9)$$

where $H_0 = H_q + H_m$ characterizes the free dynamics of the qubit and the MO with $H_q = \omega_q \sigma_z / 2$ and $H_m = \omega_m (X_m^2 + P_m^2) / 2$. The general form of the interaction term between a qubit and the MO can be modeled as

$$H_{int} = g_0 (\mathbf{n} \cdot \vec{\sigma}) X_m, \quad (10)$$

where \mathbf{n} is a normal vector in Bloch space such that

$$\mathbf{n} \cdot \vec{\sigma} = \sigma_x \cos \phi \sin \theta + \sigma_y \sin \phi \sin \theta + \sigma_z \cos \theta. \quad (11)$$

In most experimental works [25, 37], the mechanical mode only couples to the one component of the Pauli matrix, i.e., $\sigma_x X_m$ ($\phi = 0, \theta = \pi/2$). However, it is also possible to couple the mechanical motion to more than one component of the Pauli matrix due to the imperfection of the quantum circuit. An experimental realization of such model can be achieved by an electromechanical system, where a nanomechanical oscillator coupled capacitively to a Cooper-pair box (CPB) as a charge qubit operating near the so-called degeneracy point (see Fig. 1(b)) [24]. In this setup, the tiny vibration of the mechanical oscillator can modify the gate-voltage $V_g(x)$ as well as the gate-capacitor $C_g(x)$ such that the gate-charge $n_g(x) = C_g(x)V_g(x)/2e$ becomes mechanically position-dependent (see Appendix A). By controlling the sensitivity of the charge qubit with respect to the gate charge $n_g(x)$, the direct coupling between the qubit and the MO becomes possible.

For the charge qubit, the dynamics and the transition frequency ω_q are strongly dependent on gate-charge $n_g(x)$ and therefore on mechanical displacement operator x . Such dependence on the one hand could be destructive as the offset-charge can induce noise to the qubit and increases its decoherence rate. On the other hand, it induces a desirable coupling between the qubit and the mechanical modes in our model. In this case, $H_{int} = (g_x \sigma_x + g_z \sigma_z) X_m$ describes the interaction Hamiltonian where $g_y = 0$ (for $\phi = 0$) and $g_x = g_0 \sin \theta$, while $g_z = g_0 \cos \theta$ characterizes the residual coupling rate (see Appendix A).

The presence of the coupling term $g_x \sigma_x X_m$ and the additional coupling $g_z \sigma_z X_m$ at the same time, which contain the perpendicular and parallel components σ_x and σ_z , with respect to the free Hamiltonian of the qubit $H_q = \omega_q \sigma_z / 2$, make it possible to produce a coherent state for a qubit from the completely incoherent initial state (2). In addition, the presence of an additional term $g_z \sigma_z X_m$ in this case, which also contains mechanical displacement, applies the net average force on the MO. This allows the observation of the mechanical coherence in the system as well.

To quantify the quantum coherence of the qubit and the MO, we employ the measure of the l_1 -norm of coherence and define the qubit coherence as $C_q(t) = \sqrt{\langle \sigma_x(t) \rangle^2 + \langle \sigma_y(t) \rangle^2}$ and use $C_m(t) = \sqrt{\langle X_m(t) \rangle^2 + \langle P_m(t) \rangle^2}$ for the mechanical coherent displacement, respectively. The expectation values of time-dependent operators $\langle \sigma_x(t) \rangle$, $\langle \sigma_y(t) \rangle$, $\langle X_m(t) \rangle$ and $\langle P_m(t) \rangle$ are determined

through the following relations

$$\langle \sigma_{x(y)}(t) \rangle = \text{Tr} \left[\rho(t) (\sigma_{x(y)} \otimes \mathbb{I}_n) \right] = \text{Tr} \left[\rho_q(t) \sigma_{x(y)} \right], \quad (12a)$$

$$\langle X_m(t) \rangle = \text{Tr} \left[\rho(t) (\mathbb{I}_q \otimes X_m) \right] = \text{Tr} \left[\rho_m(t) X_m \right], \quad (12b)$$

$$\langle P_m(t) \rangle = \text{Tr} \left[\rho(t) (\mathbb{I}_q \otimes P_m) \right] = \text{Tr} \left[\rho_m(t) P_m \right], \quad (12c)$$

where $\mathbb{I}_n, \mathbb{I}_q$ are the identity operators for the qubit and the MO, $\rho(t)$ represents the evolved density matrix of the system, while $\rho_q(t)$ and $\rho_m(t)$ denote the reduced density matrices of the qubit and the MO, respectively. Once we compute the evolved density matrix of the system in both ideal and non-ideal situations, we can easily calculate the coherence parameters.

ACKNOWLEDGMENTS

N.E.A. acknowledges the project CZ.02.1.01/0.0/0.0/16_026/0008460 of MEYS CR. A.A.R. and R.F. acknowledge the support of the project 20-16577S of the Czech Science Foundation. R.F. also acknowledges the grant LTAUSA19099 of MEYS CR.

Appendix A: Extracting the interaction Hamiltonian of the qubit-mechanical system

To extract the interaction term, we start with the equivalent circuit of Fig. 1(d), such that the equivalent voltage $V_g(x)$, which is the voltage difference across open terminals A and B (the equivalent voltage applied across the Josephson junction), is given by (see Fig 6(a))

$$V_g(x) = V_A(x) - V_B(x) = V_{\text{dc}} \left(\frac{C_m^-(x)}{C_m^-(x) + C_0} - \frac{C_m^+(x)}{C_m^+(x) + C_0} \right), \quad (A1)$$

with

$$C_m^\pm(x) = \frac{\epsilon_0 A}{x_0 \pm x} = \frac{C_m^0}{(1 \pm x/x_0)}, \quad (A2)$$

where x_0 indicates the static separation between the parallel plate capacitors $C_m^\pm(x)$, while ϵ_0 and A represent the permittivity and area of the plate capacitors, respectively. By expanding $V_g(x)$ around small motion at $x = 0$, we have

$$C_m^\pm(x) \approx C_m^0 \left(1 \mp \frac{x}{x_0} \right), \quad (A3)$$

$$V_g(x) \approx 2V_{\text{dc}} \frac{C_m^0 C_0}{(C_m^0 + C_0)^2} \cdot \frac{x}{x_0} + \mathcal{O} \left(\frac{x}{x_0} \right)^2. \quad (A4)$$

Similarly, the equivalent capacitance $C_g(x)$ is found by replacing the DC-voltage source with a short circuit (Fig. 6 (b)),

$$\frac{1}{C_g(x)} = \frac{1}{C_{\text{eq}}(x)} = \frac{1}{C_0 + C_m^-(x)} + \frac{1}{C_0 + C_m^+(x)}, \quad (A5)$$

$$C_g(x) \approx \frac{1}{2} (C_0 + C_m^0) + \mathcal{O} \left(\frac{x}{x_0} \right)^2. \quad (A6)$$

Up to the first order in x , only the gate-voltage is linearly controlled by the mechanical displacement. Therefore, the off-set charge $n_g(x) = C_g(x)V_g(x)/2$ becomes

$$n_g(x) \approx \frac{V_{\text{dc}}}{2ex_0} \cdot \frac{C_m^0 C_0}{(C_0 + C_m^0)} x. \quad (A7)$$

The general Hamiltonian of the qubit in the presence of the mechanical motion is given by

$$H_q(x) = 4E_c \left(n - n_g(x) \right)^2 - E_J \cos \varphi, \quad (A8)$$

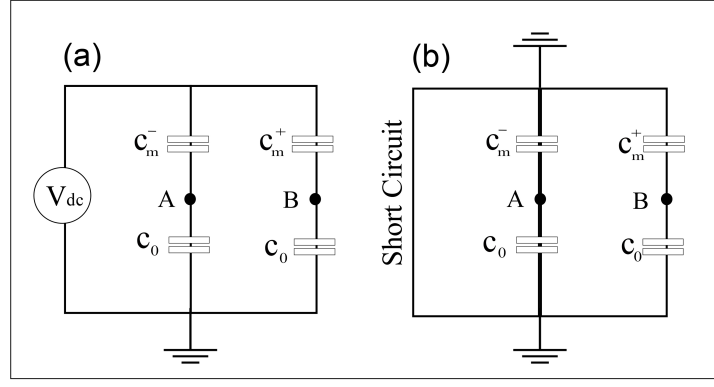


FIG. 6. (a) The Thevenin equivalent representation of the circuit in Fig. 1(c,d) for calculating $V_g(x)$, and (b) the equivalent short circuit used for calculating $C_g(x)$.

where E_c and E_J are the charging and Josephson energy, respectively, n is the Cooper-pair number operator and φ is the superconducting phase operator which can be related to the flux operator through $\varphi = 2\pi\Phi/\Phi_0$, where $\Phi_0 = h/(2e)$ is the flux quantum. In the number-operator basis the second term of Eq. (A8) can be written as

$$-E_J \cos \varphi = -\frac{E_J}{2} \sum_n (|n\rangle\langle n+1| + |n+1\rangle\langle n|). \quad (\text{A9})$$

The eigenenergies of the Hamiltonian (A8) for each n -subspace is given by

$$\lambda_{\pm}^{(n)}(x) = 4E_c (n - n_g(x))^2 + 4E_c (n - n_g(x)) + 2E_c \pm \frac{1}{2} \sqrt{E_J^2 + (4E_c)^2 (1 + 2n - 2n_g(x))^2}. \quad (\text{A10})$$

Taking the lowest two energy-levels $|n=0\rangle$ and $|n=1\rangle$ as a ground and excited states of a qubit, respectively, into account, the qubit frequency becomes

$$\omega_q(x) = \omega_q^{(0)}(x) = \sqrt{E_J^2 + (4E_c)^2 (1 - 2n_g(x))^2}, \quad (\text{A11})$$

and the Hamiltonian (A8) takes the following form

$$H_q(x) \approx 4E_c (1 - 2n_g(x)) |1\rangle\langle 1| + 4E_c n_g^2(x) \mathbb{I} - \frac{E_J}{2} (|0\rangle\langle 1| + |1\rangle\langle 0|). \quad (\text{A12})$$

Now, the interaction Hamiltonian near the charge degeneracy point $n_g \approx 1/2$ is given by,

$$H_{int} = \frac{\partial H_q}{\partial x} x \Big|_{n_g \rightarrow \frac{1}{2}} = 8E_c (n - n_g) \frac{\partial n_g(x)}{\partial x} x \Big|_{n_g \rightarrow \frac{1}{2}} \approx 8E_c [|1\rangle\langle 1| - n_g] \frac{\partial n_g(x)}{\partial x} x \Big|_{n_g \rightarrow \frac{1}{2}} \quad (\text{A13})$$

where

$$\frac{\partial n_g(x)}{\partial x} = \frac{V_{dc}}{2ex_0} \cdot \frac{C_m^0 C_0}{(C_0 + C_m^0)}. \quad (\text{A14})$$

Using the diagonal bases

$$\begin{aligned} |+\rangle &= \cos \vartheta |0\rangle + \sin \vartheta |1\rangle, \\ |-\rangle &= -\sin \vartheta |0\rangle + \cos \vartheta |1\rangle, \end{aligned} \quad (\text{A15})$$

where $2\vartheta = \pi/2 - \theta_0$ and $\theta_0 = \arctan[4E_c(1 - 2n_g)/E_J]$ [24], the Eq. (A13) can be written as

$$H_{int} = g_0 X_m \left[\cos \theta_0 \sigma_x - \sin \theta_0 \sigma_z + (1 - 2n_g) \right] \Big|_{n_g \rightarrow \frac{1}{2}}. \quad (\text{A16})$$

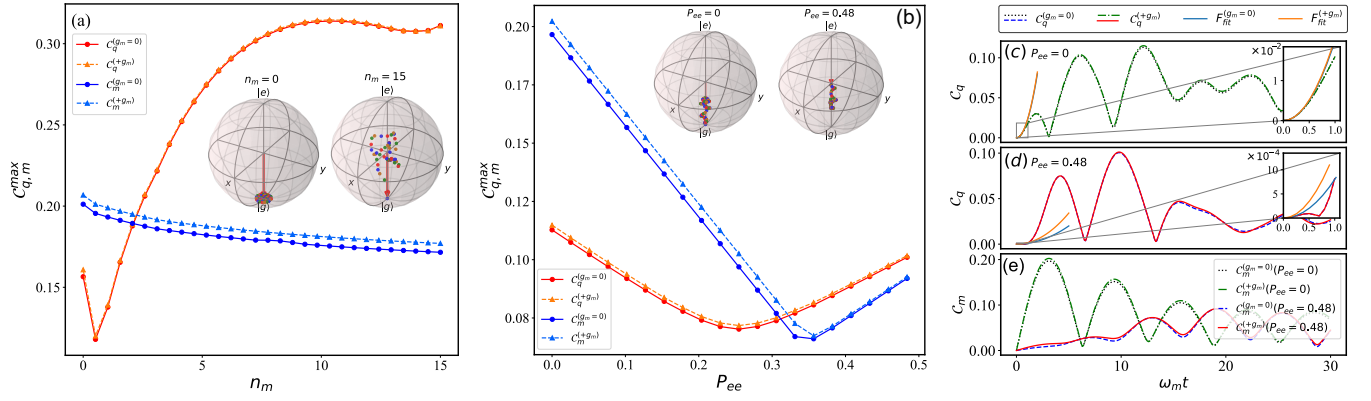


FIG. 7. Optimum values of coherence parameters as a function of (a) the mechanical occupation number n_m when $P_{ee} = 0$ and (b) the qubit probability amplitude P_{ee} when $n_m = 0.5$, in the presence and in the absence of the coupling term g_m . Inset plots in panels (a) and (b) show the evolution of the Bloch vector during $\omega_m t \in [0, 30]$ for (a) different mechanical occupation numbers $n_m = 0$ and $n_m = 15$ with $P_{ee} = 0$, as well as (b) different values of $P_{ee} = 0$ and $P_{ee} = 0.48$ with $n_m = 0.5$. The evolution of C_q for (c) $P_{ee} = 0$ and (d) $P_{ee} = 0.48$ together with the quadratic fittings in the absence and in the presence of g_m , when $n_m = 0.5$. Inset plots in panels (c) and (d) show the zoomed rectangle-region of fitting for a short time interval $\omega_m t \in [0, 1]$. (e) The evolution of C_m for two different values of $P_{ee} = 0$ and $P_{ee} = 0.48$ with and without coupling constant g_m . Other numerical parameters are the same as those in Fig. 2.

Here, we define $x = \sqrt{2}x_{zpf} X_m$ with $x_{zpf} = \sqrt{\hbar/(2m\omega_m)}$ being the zero-point fluctuation, $\sigma_z \equiv |+\rangle\langle+| - |-\rangle\langle-|$ and $\sigma_x \equiv |+\rangle\langle-| + |-\rangle\langle+|$ denote the z and x components of Pauli matrix, aligned with the energy quantization axis and perpendicular to it, respectively, and g_0 is the single phonon qubit-mechanics coupling, defined as

$$g_0 = \frac{4E_c}{2e} \cdot \frac{C_m^0 C_0}{(C_0 + C_m^0)} \cdot \frac{x_{zpf}}{x_0} V_{dc}. \quad (\text{A17})$$

By using the spherical coordinates in the Bloch space, where $\phi = 0$ and $\theta \equiv \theta_0 + \pi/2$, the general form of interaction Hamiltonian (1) is derived and the qubit-mechanical coupling rates g_x and g_z can be extracted as

$$\begin{aligned} g_x &= g_0 \cos \theta_0 = g_0 \sin \theta, \\ g_z &= -g_0 \sin \theta_0 = g_0 \cos \theta, \end{aligned} \quad (\text{A18})$$

In addition, standing close to the degeneracy point induces a small qubit-independent shift (QID) with the coupling rate $g_m = g_0(1 - 2n_g)$ to the MO which is negligible for $n_g \rightarrow 1/2$ such that we have ignored it in Eq. (1). The complete dynamical behavior of the coherence parameters in the presence of this shift has been discussed in Appendix B.

Appendix B: Effects of the coherent driving term on the quantum coherence

In the vicinity of the degeneracy point ($n_g \rightarrow 1/2$), the coupling term $g_m = g_0(1 - 2n_g)$ is too small in comparison with other coupling rates g_x and g_z so that, the QID term can slightly modify the dynamics of the quantum coherence. By considering the shift term $g_m X_m$, the interaction Hamiltonian of the system now becomes

$$H_{int} = (g_x \sigma_x + g_z \sigma_z + g_m) X_m. \quad (\text{B1})$$

In Fig. 7(a,b) the optimum values of the coherence parameters C_q and C_m with respect to the mechanical-thermal number n_m (Fig. 7(a)) and the qubit weight P_{ee} (Fig. 7(b)) are depicted in the presence and the absence of the coupling rate g_m . From those panels, we can see that the constant shift moderately improves the results for both qubit coherence and mechanical coherent displacement. In addition, the inset plots in panels (a) and (b) of Fig 7 show the evolution of the Bloch vector for different values of n_m (Fig. 7(a)) and P_{ee} (Fig. 7(b)) when we consider the coupling term $g_m \neq 0$. As is evident from inset plots of Fig. 7(a), by increasing the mechanical occupation numbers n_m , the expectations $\langle \sigma_x(t) \rangle$ and $\langle \sigma_y(t) \rangle$ take larger values which give rise to larger amount of qubit coherence parameter C_q . On the other hand, increasing the qubit thermal number n_q or equivalently, P_{ee} , causes the reduction in mean values of $\langle \sigma_x(t) \rangle$ and $\langle \sigma_y(t) \rangle$ and consequently C_q (see inset plots in Fig 7(b)). These results are completely in agreement with the previous outcomes explained in the body of the manuscript. Moreover, in Panels (c,d) and (e) of Fig. 7, the evolution of C_q and C_m in the absence and the presence of the QID term are depicted as a function of normalized

time $\omega_m t$ for two different values $P_{ee} = 0$ and $P_{ee} = 0.48$. In accordance with Fig. 7(a,b), the presence of g_m can slightly change the values of the coherence parameters in time.

Similar to what we get in Eq. (5), we can also calculate the coherence components for a very tiny time interval, when we apply QID $g_m X_m$ into the dynamics of the system

$$\langle X_m(t) \rangle \approx \sqrt{2}t^2 \left[g_z \left(\omega_m (2P_{ee} - 1)n_m (4n_m + 3) + \omega_q (n_m + \frac{1}{2}) \right) + g_m \left(\omega_m n_m (4n_m + 3) + \omega_q (2P_{ee} - 1)(n_m + \frac{1}{2}) \right) \right], \quad (\text{B2a})$$

$$\langle P_m(t) \rangle \approx -\sqrt{2}g_z t (2P_{ee} - 1), \quad (\text{B2b})$$

$$\langle \sigma_x(t) \rangle \approx 2g_x t^2 (2n_m + 1) [g_z (2P_{ee} - 1) + g_m], \quad (\text{B2c})$$

$$\langle \sigma_y(t) \rangle \approx 0. \quad (\text{B2d})$$

As is evident from Eqs. (5c) and (B2c), the qubit coherence parameter evolves quadratically in a very short time domain. By introducing the fitting function $F_{\text{fit}}^{(g_m=0)} = |2g_x g_z (2n_m + 1)(2P_{ee} - 1)t^2|$ and $F_{\text{fit}}^{(+g_m)} = |2g_x (2n_m + 1)(g_z (2P_{ee} - 1) + g_m)t^2|$ associated with the Eqn. (5c) and (B2c), in Panels (c) and (d) of Fig.7 and their insets we checked the consistency of the analytical and numerical results for qubit coherence in two conditions of the absence and the presence of the coupling rate g_m , respectively. As can be seen, for a short time interval the results are matched which confirm that qubit coherence parameter behaves quadratically for the initial time interval.

-
- [1] Vittorio Giovannetti, Seth Lloyd, and Lorenzo Maccone, “Advances in quantum metrology,” *Nature Photonics* **5**, 222–229 (2011), arXiv:1102.2318.
- [2] C. L. Degen, F. Reinhard, and P. Cappellaro, “Quantum sensing,” *Reviews of Modern Physics* **89**, 035002 (2017), arXiv:1611.02427.
- [3] Avijit Misra, Uttam Singh, Samyadeb Bhattacharya, and Arun Kumar Pati, “Energy cost of creating quantum coherence,” *Physical Review A* **93**, 052335 (2016).
- [4] Jader P. Santos, Lucas C. Céleri, Gabriel T. Landi, and Mauro Paternostro, “The role of quantum coherence in non-equilibrium entropy production,” *npj Quantum Information* **5**, 1–7 (2019).
- [5] A. Galindo and M. A. Martín-Delgado, “Information and computation: Classical and quantum aspects,” *Reviews of Modern Physics* **74**, 347–423 (2002).
- [6] T. D. Ladd, F. Jelezko, R. Laflamme, Y. Nakamura, C. Monroe, and J. L. O’Brien, “Quantum computers,” *Nature* **464**, 45–53 (2010), arXiv:1009.2267.
- [7] J. M. Matera, D. Egloff, N. Killoran, and M. B. Plenio, “Coherent control of quantum systems as a resource theory,” *Quantum Science and Technology* **1**, 01LT01 (2016).
- [8] Seth Lloyd, “Quantum coherence in biological systems,” *Journal of Physics: Conference Series* **302**, 012037 (2011).
- [9] Akihito Ishizaki and Graham R. Fleming, “Quantum Coherence in Photosynthetic Light Harvesting,” *Annual Review of Condensed Matter Physics* **3**, 333–361 (2012).
- [10] Andreas Winter and Dong Yang, “Operational Resource Theory of Coherence,” *Physical Review Letters* **116**, 120404 (2016).
- [11] Alexander Streltsov, Gerardo Adesso, and Martin B. Plenio, “Colloquium: Quantum Coherence as a Resource,” *Reviews of Modern Physics* **89**, 041003 (2017), arXiv:1609.02439.
- [12] Felix Bischof, Hermann Kampermann, and Dagmar Bruß, “Resource Theory of Coherence Based on Positive-Operator-Valued Measures,” *Physical Review Letters* **123**, 110402 (2019), arXiv:1812.00018.
- [13] Andrew Smith, Kanupriya Sinha, and Christopher Jarzynski, “Quantum Coherences and Classical Inhomogeneities as Equivalent Thermodynamics Resources,” *Entropy* **24**, 474 (2022).
- [14] Yao Yao, Xing Xiao, Li Ge, and C. P. Sun, “Quantum coherence in multipartite systems,” *Physical Review A* **92**, 022112 (2015).
- [15] Ming-Liang Hu, Xueyuan Hu, Jieci Wang, Yi Peng, Yu-Ran Zhang, and Heng Fan, “Quantum coherence and geometric quantum discord,” *Physics Reports Quantum Coherence and Geometric Quantum Discord*, **762–764**, 1–100 (2018).
- [16] Giacomo Guarneri, Michal Kolář, and Radim Filip, “Steady-State Coherences by Composite System-Bath Interactions,” *Physical Review Letters* **121**, 070401 (2018), arXiv:1802.08283.
- [17] Giacomo Guarneri, Daniele Morrone, Barış Çakmak, Francesco Plastina, and Steve Campbell, “Non-equilibrium steady-states of memoryless quantum collision models,” *Physics Letters A* **384**, 126576 (2020), arXiv:2001.01723 [cond-mat, physics:quant-ph].
- [18] Mike Reppert, Deborah Reppert, Leonardo A. Pachon, and Paul Brumer, “Equilibrium Coherence in the Multi-level Spin-boson Model,” *Physical Review A* **102**, 012211 (2020), arXiv:1911.07606 [quant-ph].
- [19] Ricardo Román-Ancheyta, Michal Kolář, Giacomo Guarneri, and Radim Filip, “Enhanced steady-state coherence via repeated system-bath interactions,” *Physical Review A* **104**, 062209 (2021).
- [20] J. D. Cresser and J. Anders, “Weak and ultrastrong coupling limits of the quantum mean force Gibbs state,” *Physical Review Letters* **127**, 250601 (2021), arXiv:2104.12606 [quant-ph].
- [21] Artur Slobodeniuk, Tomáš Novotný, and Radim Filip, “Extraction of autonomous quantum coherences,” *Quantum* **6**, 689 (2022), arXiv:2106.15721.
- [22] Federico Cerisola, Marco Berritta, Stefano Scali, Simon A. R. Horsley, James D. Cresser, and Janet Anders, “Quantum-classical correspondence in spin-boson equilibrium states at arbitrary coupling,” (2022), arXiv:2204.10874 [quant-ph].

- [23] Archak Purkayastha, Giacomo Guarnieri, Mark T. Mitchison, Radim Filip, and John Goold, “Tunable phonon-induced steady-state coherence in a double-quantum-dot charge qubit,” *npj Quantum Information* **6**, 1–7 (2020).
- [24] X. Ma, J. J. Viennot, S. Kotler, J. D. Teufel, and K. W. Lehnert, “Non-classical energy squeezing of a macroscopic mechanical oscillator,” *Nature Physics* **17**, 322–326 (2021), arXiv:2005.04260.
- [25] A. D. O’Connell, M. Hofheinz, M. Ansmann, Radoslaw C. Bialczak, M. Lenander, Erik Lucero, M. Neeley, D. Sank, H. Wang, M. Weides, J. Wenner, John M. Martinis, and A. N. Cleland, “Quantum ground state and single-phonon control of a mechanical resonator,” *Nature* **464**, 697–703 (2010).
- [26] Benjamin M. Brubaker, Jonathan M. Kindem, Maxwell D. Urmeý, Sarang Mittal, Robert D. Delaney, Peter S. Burns, Michael R. Vissers, Konrad W. Lehnert, and Cindy A. Regal, “Optomechanical ground-state cooling in a continuous and efficient electro-optic transducer,” arXiv:2112.13429 [quant-ph] (2021), arXiv:2112.13429 [quant-ph].
- [27] Rishabh Sahu, William Hease, Alfredo Rueda, Georg Arnold, Liu Qiu, and Johannes Fink, “Quantum-enabled interface between microwave and telecom light,” *Nature Communications* **13**, 1276 (2022), arXiv:2107.08303.
- [28] Robert D. Delaney, Maxwell D. Urmeý, Sarang Mittal, Benjamin M. Brubaker, Jonathan M. Kindem, Peter S. Burns, Cindy A. Regal, and Konrad W. Lehnert, “Non-destructive optical readout of a superconducting qubit,” arXiv:2110.09539 [quant-ph] (2021), arXiv:2110.09539 [quant-ph].
- [29] Ze-Liang Xiang, Sahel Ashhab, J. Q. You, and Franco Nori, “Hybrid quantum circuits: Superconducting circuits interacting with other quantum systems,” *Reviews of Modern Physics* **85**, 623–653 (2013).
- [30] S. M. Girvin, M. H. Devoret, and R. J. Schoelkopf, “Circuit QED and engineering charge based superconducting qubits,” *Physica Scripta* **T137**, 014012 (2009), arXiv:0912.3902 [cond-mat].
- [31] T. Baumgratz, M. Cramer, and M. B. Plenio, “Quantifying Coherence,” *Physical Review Letters* **113**, 140401 (2014), arXiv:1311.0275 [quant-ph].
- [32] Yu-Ran Zhang, Lian-He Shao, Yongming Li, and Heng Fan, “Quantifying coherence in infinite-dimensional systems,” *Physical Review A* **93**, 012334 (2016).
- [33] M. D. LaHaye, J. Suh, P. M. Echternach, K. C. Schwab, and M. L. Roukes, “Nanomechanical measurements of a superconducting qubit,” *Nature* **459**, 960–964 (2009).
- [34] F. Rouxinol, Y. Hao, F. Brito, A. O. Caldeira, E. K. Irish, and M. D. LaHaye, “Measurements of nanoresonator-qubit interactions in a hybrid quantum electromechanical system,” *Nanotechnology* **27**, 364003 (2016).
- [35] Yiwen Chu, Prashanta Kharel, William H. Renninger, Luke D. Burkhardt, Luigi Frunzio, Peter T. Rakich, and Robert J. Schoelkopf, “Quantum acoustics with superconducting qubits,” *Science* **358**, 199–202 (2017), arXiv:1703.00342.
- [36] Lucas R. Sletten, Bradley A. Moores, Jeremie J. Viennot, and Konrad W. Lehnert, “Resolving Phonon Fock States in a Multimode Cavity with a Double-Slit Qubit,” *Physical Review X* **9**, 021056 (2019), arXiv:1902.06344.
- [37] E. Alex Wollack, Agnetta Y. Cleland, Rachel G. Gruenke, Zhaoyou Wang, Patricio Arrangoiz-Arriola, and Amir H. Safavi-Naeini, “Quantum state preparation and tomography of entangled mechanical resonators,” *Nature* **604**, 463–467 (2022), arXiv:2110.07561.
- [38] F. Bloch, W. W. Hansen, and M. Packard, “The Nuclear Induction Experiment,” *Physical Review* **70**, 474–485 (1946).
- [39] Hugo Cable, Peter L. Knight, and Terry Rudolph, “Measurement-induced localization of relative degrees of freedom,” *Physical Review A* **71**, 042107 (2005).
- [40] Radim Filip and Petr Marek, “Thermally induced creation of quantum coherence,” *Physical Review A* **90**, 063820 (2014).
- [41] Hsiang-Yu Lo, Daniel Kienzler, Ludwig de Clercq, Matteo Marinelli, Vlad Negnevitsky, Ben C. Keitch, and Jonathan P. Home, “Spin-motion entanglement and state diagnosis with squeezed oscillator wavepackets,” *Nature* **521**, 336–339 (2015), arXiv:1412.7100 [physics, physics:quant-ph].
- [42] D. Kienzler, C. Flühmann, V. Negnevitsky, H.-Y. Lo, M. Marinelli, D. Nadlinger, and J. P. Home, “Observation of Quantum Interference between Separated Mechanical Oscillator Wave Packets,” *Physical Review Letters* **116**, 140402 (2016).
- [43] P. Rabl, P. Cappellaro, M. V. Gurudev Dutt, L. Jiang, J. R. Maze, and M. D. Lukin, “Strong magnetic coupling between an electronic spin qubit and a mechanical resonator,” *Physical Review B* **79**, 041302 (2009).
- [44] Shimon Kolkowitz, Ania C. Bleszynski Jayich, Quirin P. Unterreithmeier, Steven D. Bennett, Peter Rabl, J. G. E. Harris, and Mikhail D. Lukin, “Coherent Sensing of a Mechanical Resonator with a Single-Spin Qubit,” *Science* **335**, 1603–1606 (2012).
- [45] Xin-Ke Li, Xin-Ke Li, Sheng-Li Ma, Ya-Long Ren, Ji-Kun Xie, and Fu-Li Li, “Coupling a single NV center to a superconducting flux qubit via a nanomechanical resonator,” *JOSA B* **39**, 69–76 (2022).
- [46] Aurélien Dantan, Bhagya Nair, Guido Pupillo, and Claudiu Genes, “Hybrid cavity mechanics with doped systems,” *Physical Review A* **90**, 033820 (2014).
- [47] Benjamin Rogers, Nicola Lo Gullo, Gabriele De Chiara, G. Massimo Palma, and Mauro Paternostro, “Hybrid optomechanics for Quantum Technologies,” *Quantum Measurements and Quantum Metrology* **2**, 11–43 (2014), arXiv:1402.1195.
- [48] Najmeh Etehadí Abari, Mohammad Hossein Naderi, and Mohammad Hossein Naderi, “Generation of the mechanical Schrödinger cat state in a hybrid atom-optomechanical system,” *JOSA B* **37**, 2146–2156 (2020).
- [49] Xing-Liang Dong, Peng-Bo Li, Tao Liu, and Franco Nori, “Unconventional quantum sound-matter interactions in spin-optomechanical-crystal hybrid systems,” *Physical Review Letters* **126**, 203601 (2021), arXiv:2104.09101 [cond-mat, physics:quant-ph].
- [50] Roson Nongthombam, Ambaresh Sahoo, and Amarendra K. Sarma, “Ground-state cooling of a mechanical oscillator via a hybrid electro-optomechanical system,” *Physical Review A* **104**, 023509 (2021).
- [51] Javier Argüello-Luengo and Darrick E. Chang, “Optomechanical strong coupling between a single cavity photon and a single atom,” arXiv:2108.03526 [physics, physics:quant-ph] (2021), arXiv:2108.03526 [physics, physics:quant-ph].
- [52] V. Yogesh and Prosenjit Maity, “Quantum coherence, correlations and nonclassical states in the two-qubit Rabi model with parametric oscillator,” *Physica A: Statistical Mechanics and its Applications* **589**, 126641 (2022), arXiv:2106.06746 [quant-ph].
- [53] Svetlana A. Malinovskaya and Irina Novikova, *From Atomic To Mesoscale: The Role Of Quantum Coherence In Systems Of Various Complexities* (World Scientific, 2015).

- [54] Matteo Lostaglio, David Jennings, and Terry Rudolph, “Description of quantum coherence in thermodynamic processes requires constraints beyond free energy,” *Nature Communications* **6**, 6383 (2015).
- [55] Michał Horodecki and Jonathan Oppenheim, “Fundamental limitations for quantum and nanoscale thermodynamics,” *Nature Communications* **4**, 2059 (2013).
- [56] Kamil Korzekwa, Matteo Lostaglio, Jonathan Oppenheim, and David Jennings, “The extraction of work from quantum coherence,” *New Journal of Physics* **18**, 023045 (2016).
- [57] G. Francica, J. Goold, and F. Plastina, “Role of coherence in the nonequilibrium thermodynamics of quantum systems,” *Physical Review E* **99**, 042105 (2019).
- [58] Tan Van Vu and Keiji Saito, “Finite-Time Quantum Landauer Principle and Quantum Coherence,” *Physical Review Letters* **128**, 010602 (2022).
- [59] J. R. Johansson, P. D. Nation, and Franco Nori, “QuTiP 2: A Python framework for the dynamics of open quantum systems,” *Computer Physics Communications* **184**, 1234–1240 (2013).
- [60] J. R. Johansson, P. D. Nation, and Franco Nori, “QuTiP: An open-source Python framework for the dynamics of open quantum systems,” *Computer Physics Communications* **183**, 1760–1772 (2012).